ELSEVIER

Chemical Engineering Journal 139 (2008) 147–156

Chemical Engineering Journal

www.elsevier.com/locate/cej

Tuning the ring-opening reaction of 1,3-dimethylcyclohexane with the addition of potassium over Ir-containing catalysts

Sergio L. González-Cortés [a,b,*], Siraprapha Dorkjampa [a], Phuong T. Do [a], Zhongrui Li [a], José M. Ramallo-López [c], Félix G. Requejo [c]

[a] *School of Chemical, Biological and Materials Engineering, The University of Oklahoma, Norman, OK 73019, USA*

[b] *Laboratorio de Cinética y Catálisis, Departamento de Química, Facultad de Ciencias, Universidad de Los Andes, Mérida 5101, Venezuela*

[c] *Departamento de Física, FCE, UNLP and INIFTA-IFLP (CONICET), CC/67 1900 La Plata, Argentina*

Received 17 May 2007; received in revised form 3 August 2007; accepted 3 August 2007

Abstract

The Ir/SiO_2 and K ion-promoted Ir/SiO_2 catalysts were fully characterized and catalytically studied using the ring-opening reaction of 1,3-dimethylcyclohexane (1,3-DMCH) as a probe reaction. This reaction could take place during the catalytic process underwent either by gasoline or by diesel fuel for enhancing of octane numbers or cetane numbers (CNs), respectively. The Ir catalysts were characterized by chemisorption of CO and H_2, temperature-programmed techniques, X-ray photoelectron spectroscopy (XPS), extended X-ray absorption fine structure spectroscopy (EXAFS) and near-edge X-ray absorption fine structure (NEXAFS) spectroscopy. The addition of potassium ions to Ir/SiO_2 catalyst produce severe superficial changes that are reflected in its ability for catalyzing the ring-opening reaction of 1,3-dimethylcyclohexane and the selectivity to primary product from substituted to unsubstituted C–C cleavages. Ir dispersions slightly increased with rising K surface density up to 3.1 atoms nm^{-2}, but strongly decreased at higher K loadings due to the non-uniform decorative effect of potassium over Ir particles.

This contribution also reveals that the opening of C─C bonds at substituted or unsubstituted positions can be tuned varying the promoter loading. That is, the dicarbene reaction path typically occurs on Ir/SiO_2 catalyst, facilitating the formation of branched products through the opening of C─C bonds at unsubstituted positions. On the other hand, the metallocyclobutane intermediates become operative over K ion-promoted Ir/SiO_2 catalysts. This involves a metal atom and three C atoms to form cyclic intermediate specie that undergoes the opening of C─C bonds at substituted positions and facilitates the formation of unbranched products, which are more desirable in the production of diesel fuel.

Keywords: Ir catalysts; Selective ring-opening reactions; Potassium-promoted catalysts; Metal catalyst characterization

1. Introduction

In the United States, the Environment Protection Agency started implementing the Tier 2 Gasoline Sulfur Control Program for cleaner gasoline in 2004. This program limits the maximum sulfur level to 15 ppm by 2006. Additional specifications for minimum cetane index at 40 and maximum aromatics content at 35 vol.% will also be imposed. In order to meet the stringent environmental regulations on petroleum fuels several approaches have been proposed. For instance, a process involving two consecutive steps (i.e. initial hydrogenation of the aromatics to saturated naphthenic compounds, followed by traditional hydrocracking of the saturated rings [1] was proposed to achieve this task. However, because of its extensive overcracking, there is limited net gain in production of desirable paraffins via this route, and the improved distillate fuel quality results primarily from a combination of hydrogenation of aromatics and a concentration of paraffins in a reduced volume of distillate product. A novel approach that reduces the number of ring structures while retaining the carbon number of a product molecule through a selective ring opening (SRO) process was recently suggested [2–4]. The main goal of the SRO reaction is to keep the same carbon number as the original naphthenic compounds while converting them to more paraffinic compounds with expectedly higher CNs. However, as was pointed out [5], ring opening of only one ring of the fully hydrogenated products would not result in a substantial gain of CN compared to the initial CN of the fully hydrogenated molecule. Conversely,

* Corresponding author. Present address: Oxford Catalysts Company, 115e Milton Park, Oxford OX14 4RZ, UK.

E-mail addresses: goncor@ula.ve, sergio.gonzalez@oxfordcatalysts.com (S.L. González-Cortés).

1385-8947/$ – see front matter © 2007 Elsevier B.V. All rights reserved.
doi:10.1016/j.cej.2007.08.008

if the ring opening takes place on a catalyst that favors the breaking of substituted tertiary–secondary endocyclic C–C bond and some of the even more sterically hindered tertiary–tertiary C–C bond, the CNs of these products are considerably higher than the ones obtained via either acid catalyzed or dicarbene mechanism [6]. This analysis suggests that the only successful strategy to significantly increase CN of decalin feedstocks should be based on a precisely tailored catalyst with high selectivity towards the cleavage of substituted endocyclic C–C bonds.

There have been several mechanisms proposed to account for ring-opening reactions over metal catalysts. The most common hydrogenolysis mechanism that typically occurs on metals such as Ir and Rh is via the dicarbene intermediate. In this mechanism, the endocyclic C–C bond cleavage occurs on unsubstituted secondary C–C bonds [7–11]. Gault [12] studied the effect of metal particle size in Pt/Al_2O_3 catalysts for the ring opening of methylcylopentane. He observed that on highly dispersed Pt/Al_2O_3, there was an equal chance of breaking any endocyclic C–C bond. This finding was attributed to a π-allyl mechanism that competes with the dicarbene mechanism. On the other hand, on Pt catalysts with larger metal particles, secondary–secondary C–C bonds were preferentially broken. In order to explain the observed rupture of sterically hindered substituted tertiary–secondary C–C bond on these low dispersed Pt catalysts, a third mechanism was proposed that competes with the dicarbene mechanism, which involves a metallocyclobutane species as intermediate. A good evidence that supports this proposed was given by McVicker et al. [3] and Coq et al. [13] for the hydrogenolysis of 1,2,4-trimethylcyclohexane and 2,2,3,3-tetramethylbutane, respectively.

Considering the fact that a successful strategy to improve CN of feedstocks should be based on a precisely tailored catalyst with high selectivity towards the cleavage of substituted endocyclic C–C bonds and also that the metallocyclobutane adsorption mode rather than the dicarbene and/or π-allyl mechanisms can meet this target. We explore the employ of an alkali metal (potassium) to modify the catalytic properties of silica-supported iridium catalysts for selective ring-opening reaction. Indeed, this approach has been employed for Hoost and Goodwing to decrease the apparent activation energy and increased the apparent hydrogen reaction order for ethane hydrogenolysis of potassium-promoted SiO_2-supported Ru catalysts [14]. Kazi et al. [15] decreased the H_2 adsorption strength and enhanced CO adsorption when Pd/SiO_2 was modified with Li ions. Furthermore, the hydrogenation and hydrogenolysis activities were decreased with increasing Li loadings. Most recently, Pedrero et al. [16] studied the oxidation of CO in H_2-CO mixtures using alkali promoter-modified Pt/SiO_2 catalysts. They found that alkali cations (e.g. Na, Rb, Cs) not only improved the metal dispersion and titrated silanol groups (Si–OH), but also inhibited spillover-mediated H_2 oxidation pathways that decreased CO oxidation. From these results we can envisage that the addition of alkali ions to SiO_2-supported metal catalysts not only changes the hydrogen transfer reactions, but also the ensemble of atoms (metal dispersion). This might affect the adsorption mode of the model molecule and therefore the reaction pathways.

In recent publications and a series of patents, McVicker and co-workers [3,17–19] reported the high ring opening activity of Ir catalysts on six-member ring naphthenics. They pointed out the propensity of Ir to cleave C–C bonds via the dicarbene mechanism. Most recently, it was reported that the preferred pathway of ring opening of 1,2- and 1,3-dimethylcyclohexane on TiO_2-, Al_2O_3- and SiO_2-supported Ir catalysts appears to be related to a support effect rather than to an effect of metal dispersion [20]. In the present paper, to enhance CN we attempt to maximize the cleavage of substituted C–C bonds using Ir-based catalysts. We explore the effects of potassium loadings as promoter in order to determine its impact on the ring-opening reaction of 1,3-dimethylcyclohexane as model reactant. We also fully characterized the series of catalysts in order to gain insight into the relationship between the catalyst surface properties and the selectivity to ring opening products of Ir-containing catalysts.

2. Experimental

2.1. Catalyst preparation

A series of SiO_2 supported 1 wt.% Ir-containing catalysts promoted with different loadings of potassium were prepared by incipient wetness co-impregnation. Silica was impregnated with aqueous solutions of $IrCl_3 \cdot 3H_2O$ (Alfa-Aesar, 99.9%) and potassium carbonate (J.T. Baker, 99.5%) containing 1 wt.% Ir and variable K loadings. The support material was silica (HiSil-210; PPG) with a BET surface area of 250 $m^2\ g^{-1}$. After impregnation, the catalyst precursors were dried overnight at 393 K and then calcined at 573 K for 2 h in flowing air.

2.2. Catalyst characterization

2.2.1. Elemental analysis

Semi-quantitative elemental ratio was verified by energy-dispersive X-ray spectroscopy (EDXS) in fairly good agreement with the nominal composition, using a Kevex model Delta-3 system connected to a JEOL JSM-880 scanning electron microscopy. The emission peaks from the regions related to O(Kα), Si(Kα), K(Kα) and Ir(Lα) were recorded for each sample.

2.2.2. Chemisorption of CO and H_2

Reversible and irreversible H_2 or CO uptakes at 300 K were measured by the volumetric technique. Catalysts (ca. 0.50 g) were treated in H_2 at 723 K for 2 h and then evacuated at the same temperature for 0.5 h before the chemisorption measurements were obtained. After treatment, the samples were cooled to 300 K, and the first chemisorption isotherm was measured at 1–100 Torr. A second isotherm was obtained after the sample was evacuated at 300 K for 0.5 h. These two isotherms were extrapolated to zero adsorbate pressure and their difference was defined as the irreversible chemisorbed H_2 or CO and used to calculate the reported H(or CO)/Ir values.

2.2.3. Temperature-programmed reduction (TPR)

The samples were pre-treated before analyzing with a 25 cm^3 min^{-1} dry air flow rate to 573 K for 1 h. The TPR profiles were carried out by passing a continuous flow of 5 vol.% H_2–Ar mixture over approximately 100 mg of *in situ* pretreated catalysts at a flow rate of 20 cm^3 min^{-1}. The temperature was linearly increased at a heating rate of 10 K min^{-1}. The hydrogen uptake change against the temperature was monitoring using a thermal conductivity detector (TCD), SRI model 110 TCD. The detector was calibrated for hydrogen consumption using known amounts of Co_3O_4 (from Alfa Aesar, 99.7%) and relating the peak area to hydrogen uptake, taking into account the stoichiometric ratio of the reduction reaction.

2.2.4. Temperature-programmed surface reaction (TPSR)

TPSR experiments were carried out in a micro-reactor coupled to a quadrupole mass spectrometer (MKS, PPT 4.24) following carbon dioxides desorption. In a typical experiment, 50–100 mg of the sample is placed in a quartz micro-reactor and reduced with flowing hydrogen (50 cm^3/min) to 723 K for 60 min. The temperature was linearly increased at a heating rate of 10 K/min. The sample is then purged with He for 30 min at the same temperature and subsequently cooled up to 300 K under flowing He. CO adsorption was conducted using 5 cm^3 loop pulses of 5% CO-He until saturating the metal surface. This was confirmed, monitoring the CO partial pressure ($m/z = 28$) with quadrupole mass spectrometer. The samples is finally heated up to 1023 K under He flow (50 cm^3/min), keeping the sample at this temperature for 1 h. A similar proceeding for basicity measurements was used, however the samples were pretreated with flowing air and the adsorbate was carbon dioxides instead of carbon monoxide.

2.2.5. X-ray photoelectron spectroscopy (XPS)

X-ray photoelectron spectroscopy data were recorded at room temperature on a Physical Electronics PHI 5800 ESCA System with monochromatic Al Kα X-rays (1486.6 eV) operated at 100 W and 15 V in a chamber pressure of approximately 2.0×10^{-9} Torr. A 400 μm spot size and 58.7 eV pass energy were typically used for the analysis. Sample charging during the measurement was compensated by an electron flood gun. The electron take-off angle was 45° with respect to the sample surface. The reduction or the reaction of the samples was performed in a packed bed micro-reactor with an on/off valve on the top and bottom of the reactor. The reactor with the sample under He was transferred to a glove bag; the sample (in powder form) was placed in a stainless steel holder and it was kept in a vacuum transfer vessel (model 04-110A from Physical Electronics) to avoid any exposure to the atmosphere before the analysis. The energy scale of the instrument was calibrated using the Ag $3d_{5/2}$ line at binding energy of 368.3 eV. The XPS data from the regions related to the C (1s), O (1s), Ir (4f), K (2p) and Si (2p) core levels were recorded for each sample. Quantification of the surface composition was carried out by integrating the peaks corresponding to each element with aid of the Shirley back ground subtraction algorithm, and then converting these peak areas to atomic composition by using the sensitivity factors provided for each element by the PHI 5800 system software.

2.2.6. Ir L_3-edge X-ray absorption spectroscopy

Extended X-ray absorption fine structure (EXAFS) and near-edge X-ray absorption fine structure (NEXAFS) spectra of the Ir L_3 edge (11,215 eV) were recorded at the 2.3 beamline of the SSRL (Stanford Synchrotron Radiation Laboratory) in transmission mode using a Si(1 1 1) double-crystal monochromator. Spectra were taken using an *in situ* cell, which has been described previously [21,22]. Samples were held within a 0.8-mm i.d. quartz capillary with 0.1-mm-thick walls. Gases were metered with electronic mass flow controllers. Ir catalysts were exposed to H_2 at 723 K, and reduction process was monitored from X-ray absorption near-edge spectra (XANES); we determined the extent of reduction by monitoring changes in the white line intensity. When the intensity of the white line remained unchanged, catalyst was cooled down to room temperature in H_2 and EXAFS spectra were taken.

2.2.6.1. EXAFS data processing. The fine structure oscillations of each spectrum were isolated using the ATHENA program [23]. The data were then fitted using the ARTHEMIS program [23] in *R*-space between 1.8 and 3.1 Å to determine interatomic distances and coordination numbers. Backscattering amplitudes and phase shifts of theoretical standards were generated with the use of FEFF6.0 [24] algorithm. As an *ab initio* calculation, FEFF uses a list of atomic coordinates in a cluster and physical information about the system, such as type of absorbing atom and excited core-level for its calculation. In our case, the list of atomic coordinates was simplified using ATOMS [25] which generates the required coordinates starting from a crystallographic description of the metallic Ir system.

2.3. Catalytic activity measurement and data analysis

The ring-opening reaction of 1,3-dimethylcyclohexane (DMCH) (obtained from Sigma–Aldrich, 99%) was conducted at 593, total pressure of 3540 kPa and molar ratio of hydrogen/hydrocarbon of 30. The runs were carried out in a plug-flow reactor consisting of a 0.5 in. stainless steel tube placed inside an electric furnace equipped with a three-zone temperature controller. In all runs, the catalyst bed was kept isothermal. Hydrogen and liquid hydrocarbon were brought in contact in the co-current mode. The liquid was continuously fed into the reactor using an Isco LC-5000 high-pressure syringe pump operating in the volumetric flow rate range of 0.15–400 mL/h. Before each run, the catalyst was reduced in hydrogen flow at 723 K for 2 h and then cooled to the reaction temperature (593 K). Dehydrogenated compounds (xylenes), coke and deep hydrogenolysis products (e.g., C1, C2), detected on the ring opening of naphthenics over Ir catalysts conducted at atmospheric pressure [26], were not observed in the current study. In fact, this study was conducted at high pressure, high hydrogen/hydrocarbon ratio and negligible catalyst deactivation.

Table 1
Compositions, metal dispersions and CO_2 adsorbed by the potassium-promoted 1 wt.% Ir/SiO_2 catalysts

K loading[a] (atoms nm^{-2})	Catalyst	CO/Ir[b]	H/Ir[b]	N_{Ir-Ir}[c]	d_p[c] (nm)	CO_2[d] ($\mu mol/g_{cat}$)
0	Ir/SiO_2	0.58	0.40	11.3	7.4	0.55
0.10	Ir–0.1K/SiO_2	0.43	–	–	–	–
0.51	Ir–0.5K/SiO_2	0.61	1.13	10.8	4.2	1.3
1.3	Ir–1.3K/SiO_2	0.66	–	–	–	–
2.1	Ir–2K/SiO_2	0.66	1.50	9.6	2.0	1.8
3.1	Ir–3K/SiO_2	0.70	–	–	–	4.0
5.1	Ir–5K/SiO_2	0.52	0.30	–	–	12.4

[a] Per nm^2 of SiO_2 measured by BET method.
[b] Chemisorption data obtained at 300 K after reducing the samples at 723 K.
[c] Average coordination number (N) and metal particle size (d_p) determined by EXAFS.
[d] Chemisorption data obtained from the samples oxidized at 723 K.

The products were collected in a dry ice in acetone bath. The liquid product was manually injected into a Hewlett-Packard 5890 Plus GC for composition analysis. A Shimadzu GC-MS-QP5000 was used to identify the products with maximum certainty and standard compounds were used to confirm the identity of the compounds.

3. Results and discussion

3.1. Metal dispersion and particle size of Ir catalysts

Compositions and metal dispersions of the potassium ions-promoted Ir catalysts are listed in Table 1. For SiO_2-supported catalysts, Ir dispersions slightly increased with increasing K^+ surface density (0–3.1 atoms nm^{-2}) as the average Ir–Ir coordination number and hence the particle size decreased. However, higher K^+ loadings (i.e. 5.1 atoms nm^{-2}) produced a diminution in Ir dispersion. As one expected, the catalysts with lower particle sizes had higher hydrogen and CO uptakes than those modified with large potassium loading, as a consequence of the blocking effect of potassium on Ir particles. Indeed, it has previously been reported that alkali ions improves metal dispersions [27–29] but electrostatic arguments do not account for the higher metal dispersions achieved on alkali-modified SiO_2 [16]. Measurements of basicity, on the other hand, follow the expected trend. That is, the CO_2 uptakes increase with rising potassium ion loadings. Particularly notable is the sample with the highest content of potassium (5.1 atoms nm^{-2}), suggesting the presence of a high surface density of potassium ion on silica surface.

3.2. Temperature-programmed techniques

In order to find out the potassium-promoter effect on the reducibility of Ir/SiO_2 catalysts we characterized those samples by temperature-programmed reduction and the results are illustrated in Fig. 1. The TPR profile of the unmodified Ir/SiO_2 catalyst shows two hydrogen-consumption steps (Fig. 1a), a shoulder at 534 K and a main feature at 605 K. They are attributed to the reduction of different nano-aggregate states of IrO_x species on the silica surface [30] or two morphologically different particles of iridium oxide [31]. When rising K loadings up to 1.3 atoms nm^{-2}, the major reduction step was shifted to lower reduction temperatures. Further promoter loadings caused an opposite behavior on this peak position. On the other hand, a small hydrogen uptake at higher temperatures (above ~740 °C) did become not only more intense with increasing potassium loading, but also more complex since several reduction steps were defined in the TPR profile of 5.1 atoms nm^{-2} modified-Ir/SiO_2 catalyst (see Fig. 1g). The dependence of the major reduction steps with potassium content indicates that low loadings of potassium markedly promote the reducibility of iridium oxide, probably due to a K-O-Ir interaction that facilitates the dissociative adsorption of hydrogen. Indeed, this promoter effect of potassium ions on the reducibility of metal oxides has been previously reported [32,33]. However, potassium contents larger than 1.3 atoms nm^{-2} block most of the IrO_x clusters and therefore inhibit the reaction of reduction, requiring higher temperatures for reducing the oxide particles.

Quantitative data extracted from the TPR profiles and represented as inset in the upper right side of Fig. 1 shows an increase

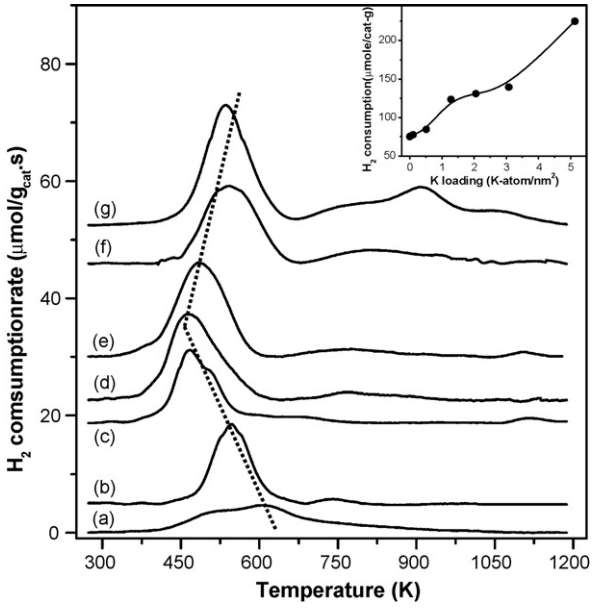

Fig. 1. Temperature-programmed reduction profiles of the catalytic precursors of K^+-promoted Ir/SiO_2 catalysts. (a) $1Ir/SiO_2$, (b) 1Ir–0.1K/SiO_2, (c) 1Ir–0.5K/SiO_2, (d) 1Ir–1.3K/SiO_2, (e) 1Ir–2K/SiO_2, (f) 1Ir–3K/SiO_2, (g) 1Ir–5K/SiO_2. Inset: Variation of the total H_2 consumption vs. K loadings.

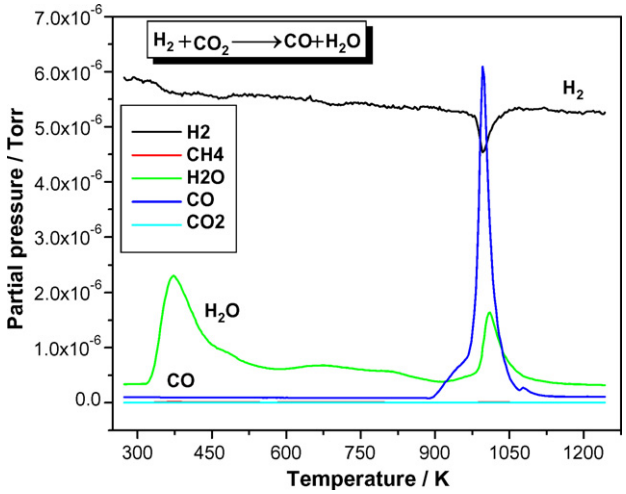

Fig. 2. Temperature-programmed reduction profile monitored by mass spectrometry of 5 atoms nm^{-2}-promoted Ir/SiO_2 catalyst.

of the total hydrogen uptake as rising potassium loadings, particularly for the catalyst with the highest content of potassium (5.1 atoms nm^{-2}). The unmodified Ir/SiO_2 catalyst and the promoted with low potassium content (i.e. 0–0.51) yielded a ratio of H_2 moles consumed per mol of Ir (H_2/Ir) close to 1.5 (i.e. 1.4–1.6) in line with the reduction of Ir(III) to metallic iridium, whereas the catalysts with larger K loadings presented H_2/Ir molar ratios greater than two (i.e. 2.4–4.3). Since it is not expected the reduction of potassium cation under the TPR analysis conditions [33,34], the excesses of hydrogen uptakes relative to the reduction of Ir(IV) (i.e., H_2/Ir molar ratios of 2.0) are attributed to the hydrogen consumption upon water–gas shift reaction (1):

$$H_2 + CO_2 \rightarrow CO + H_2O \quad (1)$$

Indeed, TPR experiment for Ir–5K/SiO_2 catalyst followed by mass spectrometry (MS), shows that the formation of carbon dioxide and water start evolving simultaneously at the same temperature that a strong hydrogen consumption is observed (ca. 1000 K), Fig. 2, indicating that the reaction (1) is the main driving force for the high hydrogen uptake at temperature above 750 K. The presence of carbon dioxide is probably due to the un-complete decomposition of potassium carbonate upon *in situ* thermal treatment under flowing air at 573 K. Therefore, the CO_2 produced at higher temperature, upon TPR experiment, reacts with hydrogen to produce carbon monoxide and water (reaction (1)).

In order to find out the reactivity of iridium cluster and potassium ions with carbon monoxide we conducted experiments of temperature-programmed surface reaction (TPRS) under helium flow. An interesting feature of these samples is the formation of large amounts of CO_2 accompanied by a poor desorption of CO, suggesting a high reactivity of Ir towards CO transformation. The CO_2 formation profiles from potassium-promoted Ir/SiO_2 catalysts are shown in Fig. 3. A major CO_2 peak centered at approximately 650 K, whose intensity increases whereas rising K ion loading up to 2.1 atoms nm^{-2}, is clearly observed. At above K compositions, the major CO_2 peak is shifted to higher temperatures whereas its intensity did not change markedly, suggesting that Ir clusters, partially blocked by potassium ions, require higher temperatures to convert CO to CO_2. Smaller CO_2 peaks at temperatures below 450 K and above 800 K are also displayed, owing to the different aggregation states of iridium. These findings indicate that the addition of potassium to Ir/SiO_2 catalyst (up to 2.1 atoms nm^{-2}) markedly promotes CO conversion to CO_2. However, catalysts with higher K compositions require higher temperatures to activate CO, owing to the partial coverage of the supported Ir clusters with K ions.

Under the pretreatment conditions of the samples, carbon dioxides can be mainly produced either by disproportionation of CO (i.e. Boudouard reaction):

$$2CO \rightarrow CO_2 + C \quad (2)$$

or the reaction of CO with hydroxyl groups from the support or promoter:

$$CO + 2OH^- \rightarrow CO_2 + H_2 + O^{2-} \quad (3)$$

Indeed, CO desorption was accompanied not only by the production of CO_2, but also by H_2 formation (reverse water–gas shift reaction). Both products started evolving simultaneously and reaching a similar temperature with maximum rate of desorption, suggesting that the main pathway of CO_2 formation is the reaction of CO with superficial hydroxyl groups (3), which is catalyzed by potassium-promoted Ir clusters. This pathway is also the main responsible for the formation of CO_2 when CO interacts with Rh/Al_2O_3 [34]. Furthermore, the total CO_2 produced at high K ion loadings coincided with the CO uptakes determined by chemisorption in line with the stoichiometric ratio of Eq. (3). In fact, studies of the transformation of CO to CO_2 over silica-supported metals have revealed that the formation of CO_2 is strongly dependent not only upon the metal supported, but also upon the promoter–chemical nature [35,36].

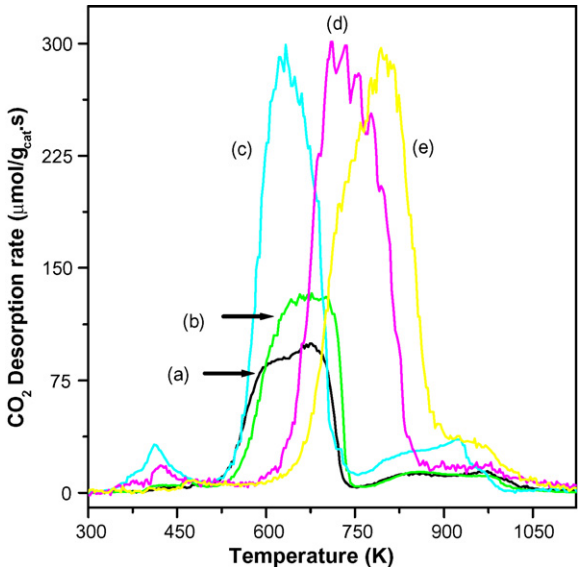

Fig. 3. Temperature-programmed surface reaction of carbon monoxide over K^+-promoted Ir/SiO_2 catalysts. (a) $1Ir/SiO_2$, (b) 1Ir–0.5K/SiO_2, (c) 1Ir–2K/SiO_2, (d) 1Ir–3K/SiO_2, (e) 1Ir–5K/SiO_2.

Table 2
Electron binding energies of the core levels for Ir 4f, K 2p and Si 2p in the K ion-promoted Ir/SiO_2 catalysts

Catalyst (wt.%)	Binding energies (±0.1 eV)			
	Ir $4f_{7/2}$	K $2p_{3/2}$	Si 2p	O 1s
$1Ir–0K/SiO_2$	60.5	–	102.3	531.9
$1Ir–0.1K/SiO_2$	60.3	292.5	102.0	531.4
$1Ir–0.5K/SiO_2$	60.4	292.7	102.2	531.5
$1Ir–1.3K/SiO_2$	60.2	292.6	102.0	531.4
$1Ir–2K/SiO_2$	60.3	292.7	102.1	531.4
$1Ir–3K/SiO_2$	60.2	292.5	102.0	531.5
$1Ir–5K/SiO_2$	60.2	292.6	102.0	531.6

3.3. X-ray photoelectron spectroscopy (XPS)

Binding energies (BEs) of core-level electrons and metal surface composition were obtained by XP spectroscopy. Table 2 summaries the observed binding energies of core levels for the studied catalyst series. The BE for Ir $4f_{7/2}$, Si 2p and O 1s peaks in the unpromoted Ir/SiO_2 catalyst are into the range of expected values for the corresponding Ir(0) and SiO_2 [37]. On the other hand, the addition of potassium produced a slight BE shift towards lower values of approximately 0.1–0.3 eV for Ir $4f_{7/2}$ and 0.3–0.5 eV for O 1s with respect to the unpromoted catalyst, whereas a BE shift towards higher values of approximately 0.4–0.6 eV for K $2p_{3/2}$ peak is illustrated, considering a BE for K $4p_{3/2}$ of 292.1 eV for 2 wt.% K/SiO_2. This trend suggests that a slight increase of electron density on the Ir clusters occurred, probably due to electron transfer from potassium oxide to Ir cluster. The presence of potassium oxide rather than K_2CO_3 is supported by the stoichiometric consumption of hydrogen at relatively low potassium loadings. However, no systematic deviation of the different binding energies with changing of potassium loadings was noted, likely due to an additional decoration effect of the K ions on the Ir nanoparticles as was previously observed for sodium ion-promoted Pd/SiO_2 catalysts [38,39].

It has been reported that metal to support atomic ratio obtained through XP spectra for supported metal catalysts can provide important information regarding the dispersion and even crystal size-morphology of the supported phase [40]. For Ir-containing catalysts, XP spectroscopy has been employed for studying the effect of the support, reduction temperature and addition of promoters on the hydrogenation reactions [41,42], however there have been no reports about the influence of alkali metal ions on the metal dispersion. The Ir $4f_{7/2}$/Si 2p, K $2p_{3/2}$/Si 2p and K $2p_{3/2}$/Ir $4f_{7/2}$ atomic surface ratios are fairly similar to the bulk atomic ratios, indicating that the catalyst components are well distributed. The atomic surface ratios linearly increase with rising K ion loading, Fig. 4, because of higher concentration of the supported species on the silica surface. Furthermore, the Ir $4f_{7/2}$/Si 2p ratio presented a change of slop from 3.1 K-atoms nm^{-2} (Fig. 4a). This trend suggests, in line with chemisorption measurements and EXAFS results (Table 1), that the addition of potassium improves the dispersion (or re-dispersion) of Ir clusters. However, potassium loading of 5.1 K-atoms nm^{-2} attenuates the peak-intensity ratio owing to a severe decoration effect of K ions over Ir clusters. This was reflected on poor metal dispersion and large CO_2 uptake (Table 1). The above also suggests that for K loadings below 3.1 atoms nm^{-2}, the CO_2 uptakes are strongly hindered due to the interaction KO_x moisture–Ir nanoparticles. Additionally, it is well-established that alkali metal ions titrate silanol (Si–OH) groups [16] and consequently their basic properties might be further hindered.

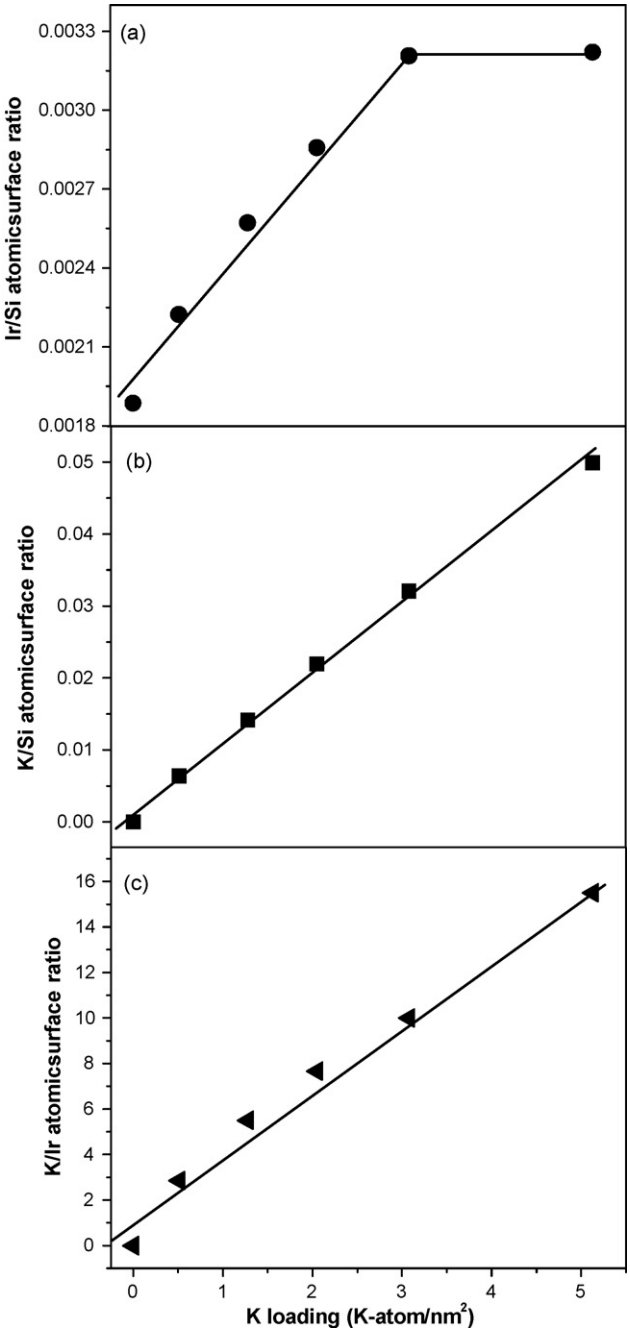

Fig. 4. Atomic surface ratios determined by X-ray photoelectron spectroscopy of promoted Ir/SiO_2 catalysts as a function of K ion loading.

3.4. Ir L_3-edge X-ray absorption spectroscopy

The Fourier transform intensities of the weighted EXAFS functions $k^3\chi(k)$ are shown in Fig. 5 for K^+-promoted Ir/SiO_2 catalyst series. The higher-shell features are similar to iridium foil thus indicating the possible existence of clustered Ir atoms. All Fourier transformed spectra are consistent with an *fcc*-structure retained in the nano-particles. The Fourier transform is an offset radial distribution diagram of the atoms surrounding the central absorber and is calculated from the interference pattern of the X-ray photoelectron wave as it passes through the crystal media. As the Fourier transform is scaled to the coordination number this makes it possible to then visually determine changes in the chemical state through observing the changes in intensity. In the EXAFS analysis the finite nanoparticle size is reflected in the reduced average coordination number resulting from their considerable surface-area-to-volume ratio. As shown in Table 3, the Ir clusters in the supported samples have a reduction of Ir–Ir coordination number as a function of K-loading. Due to the small variation of the coordination number at nano-cluster diameters larger than 2 nm and the errors associated with the EXAFS coordination number only approximate information about nano-cluster sizes can be obtained by EXAFS and thus other measurements are essential for a comprehensive characterization of the nano-clusters as a function of size. With a hemispherical cuboctahedron *fcc* model [43], the Ir particle size can be roughly estimated to be about 3.7 nm for Ir/SiO_2, 2.2 nm for 0.5 K-atoms nm^{-2}-promoted Ir/SiO_2 and 0.9 nm for 2.1 K-atoms nm^{-2}-containing Ir/SiO_2, respectively. This intensity reduction is predominantly caused by the decrease in the average first shell coordination number that results from the changing ratio of surface to bulk-like atoms in the clusters. It is clear that there is a striking decrease in Ir cluster size with increasing K loading in line with the above-mentioned trend of the metal dispersion.

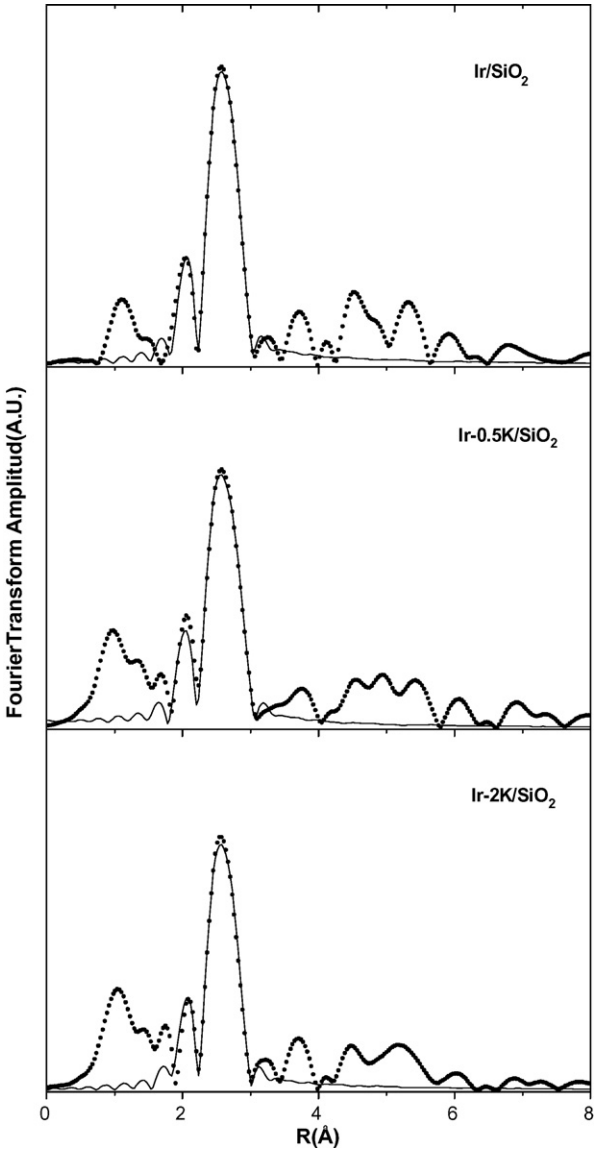

Fig. 5. Amplitude of the Fourier transforms of EXAFS data of samples measured in H_2 at RT after reduction at 723 K (●). Solid lines show the corresponding Fourier transforms of the fitted functions.

Table 3
Structural parameters of iridium obtained from fitting of EXAFS data using theoretical references developed with FEFF

Catalyst	$\langle N\rangle$[a]	R[b] (Å)	σ^{2}[c] (Å^{-2})	E_0[d] (eV)
Ir/SiO_2	11.3 ± 1	2.709(8)	0.0047(8)	7.3 ± 1
Ir–0.5K/SiO_2	10.8 ± 1	2.703(5)	0.0049(5)	7.5 ± 1
Ir–2K/SiO_2	9.6 ± 1	2.702(4)	0.0050(5)	7.0 ± 1

[a] Average coordination numbers.
[b] Bond distances.
[c] Debye–Waller factors.
[d] E_0 shift.

Additionally, a significant bond length contraction with respect to the Ir foil can be observed, the first Ir–Ir coordination bond distances shrink with increasing K loading. The relative first nearest Ir–Ir length contraction changes as a function of the inverse nano-cluster diameter. It should be noted that the bond lengths obtained from EXAFS results are average. The noticeable decrease in lattice constants of supported Ir cluster can be understood in terms of a simple liquid drop model [44] where enhanced surface energy is a main reason for the contracted lattice (nanosize effect). In response to the compressive tension, the atomic positions of the surface atoms should shift away from ideal sites and toward the cluster's core. Therefore, these surface atoms should have shorter the first Ir–Ir coordination distance [45]. These results suggest that addition of K might wet the SiO_2 surface through an anchoring effect of the silanol groups with K ions and consequently the dispersion of Ir on SiO_2 surface enhances, owing to the KO_x moisture–Ir interaction.

3.5. Catalytic activity of K ions-promoted Ir/SiO_2 catalysts

The ring-opening reaction of 1,3-DMCH produces three primary products: 2-methylheptane (2-MC7) and 4-methylheptane (4-MC7) from the breakage of tertiary–secondary C–C bonds (a and b) and 2,4-dimethylhexane (2,4-DMC6), which is formed by cleavage of a secondary–secondary C–C bond, Scheme 1.

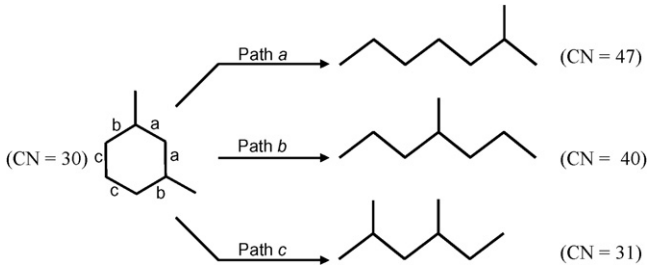

Scheme 1. Cetane numbers and reaction pathways for the primary product formation in the iridium-catalyzed ring-opening reaction of 1,3-dimethylcyclohexane.

In a recent contribution, it was predicted the CNs of such as products indicated by a, b, and c (47, 40, and 31, respectively) among many others, using artificial neural network and a database of all the available experimental CN data [5]. These estimations indicate that highly branched molecules (i.e., high CH_3/CH_2 ratio) present low CNs [46]. Since 1,3-DMCH has a CN of 30, selective cleavage at both the a and b positions (particularly at a), but not at c, would result in high CN desirable products.

Fig. 6 displays the influence of the K ion loadings on the ring-opening reaction of 1,3-DMCH. It is found that the increase of K^+ content lineally inhibits the 1,3-DMCH conversion, owing to a gradual deactivation process with increasing promoter loading. But simultaneously increases the selective ring-opening reaction, reaching a maximum selectivity when K^+ loading is about 2.1-atoms nm^{-2} and then decreasing for greater K ion contents. Even though this trend is most probably affected by the no isoconversion condition, the above-mentioned results for the unpromoted and 2.1 K-atoms nm^{-2}-promoted Ir/SiO_2 catalysts clearly evidence the strong promoter effect of potassium on silica-supported Ir catalysts. This effect is also reflected upon the primary product distribution, Fig. 7, where both the (2-MC7 + 4-MC7)/2,4-DMC6 and 2-MC7/4-MC7 ratios show

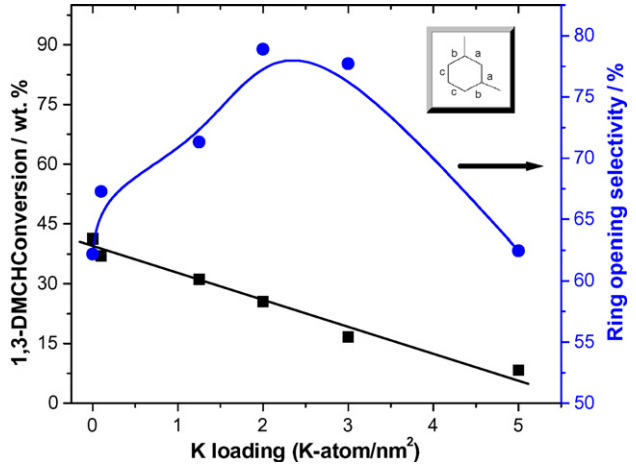

Fig. 6. Influence of the potassium ion loadings on the 1,3-DMCH conversion and ring opening selectivity over Ir/SiO_2 catalyst. Reactions were conducted at 593 K, total pressure of 3540 kPa and molar ratio of hydrogen to hydrocarbon was kept at 30. Error data ca. 5%.

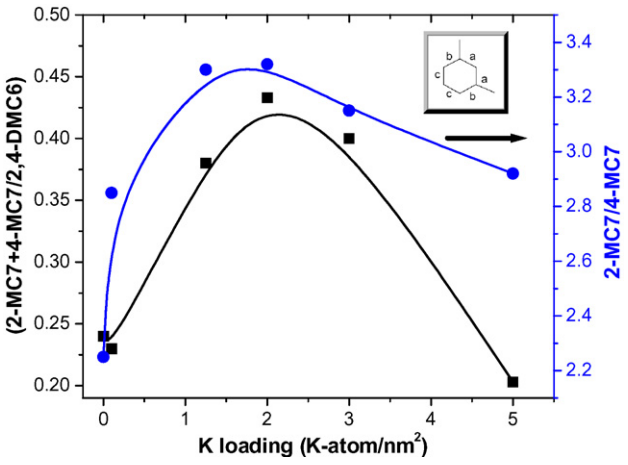

Fig. 7. Effect of the potassium ion loadings on the ratios of primary products from substituted C—C rupture to unsubstituted C—C cleavage (i.e. 2-MC7 + 4-MC7/2,4-DMC6) and substituted C—C cleavage at internal to external positions (i.e. 2-MC7/4-MC7) of Ir/SiO_2 catalyst. Reactions were carried out at 593 K, 3540 kPa and molar ratio of hydrogen to hydrocarbon of 30. Error data ca. 5%.

a similar behavior than the ring opening selectivity. However, the maximum for *a*/*b* ratio underwent a less severe change with potassium composition greater than 2 K-atoms nm^{-2}, compared with $(a+b)/c$ ratio. This trend is mainly due to the strong increase of the undesirable 2,4-DMC6 primary product compared with 2,4-MC6 and 4-MC7 at above potassium loading. No isomerization products were observed owing to the low isomerization activity of non-acidic carrier-supported Ir catalysts [47,48].

The above-mentioned catalytic results illustrate that not all ring opening products exhibit high CNs. Hence, it is very important not only the control of the specific type of C–C bond cleaved, but also the inhibition of the secondary reactions in order to reach a maximum selectivity to the desirable products. Three different ring opening adsorption modes might operate upon the synthesis of products with higher or lower CN than the original naphthalene-derived molecule: (1) π-Adsorbed olefin mode, which requires a flat adsorption of three neighboring carbon atoms. (2) Metallocyclobutane adsorption mode that involves a metal atom and three C atoms to form a cyclic intermediate. Both mechanisms can achieve C–C cleavage at substituted positions [12,49], eliminating branching and enhancing the CN. (3) Dicarbene mechanism, on the other hand, requires metal–carbon bonding of two carbon atoms and results in C–C cleavage of unsubstituted secondary–secondary carbon atoms [12]. This facilitates the formation of highly branched isoparaffins with low CNs.

Considering the above statement and the product distribution we can envisage that the main adsorption modes of 1,3-DMCH on K-promoted silica-supported Ir catalysts are the dicarbene and the metallocyclobutane mechanisms (Scheme 2). The π-adsorbed olefin mode seems not operate under the used reaction conditions, since the selectivity to primary products is far to statistical ratio owing to the absent of a flat lying adsorbed species with approximately equal accessibility of both ring C–C bonds to the surface active centers. This is most probably due to the

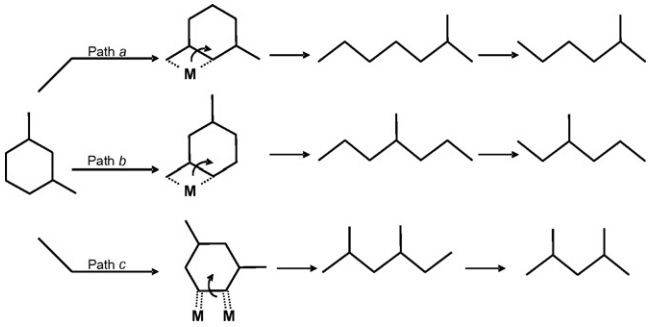

Scheme 2. Catalytic pathways of iridium-catalyzed ring opening of 1,3-DMCH and secondary hydrogenolysis reactions. Path a and b: metallocyclobutane adsorption mode, path c: dicarbene mode.

sterically hindered effect occasioned by the two bulky methyl groups present in the cyclic molecule.

There are not evidences for ring-contraction reaction from C6 to C5 rings in line with a previous report [20]. According to Gault and coworkers [49], the reaction path involving the metallocyclobutane intermediate would have activation energy higher than that operating the dicarbene intermediate. However, the ring-opening reaction of 1,3-DMCH through the metallocyclobutane adsorption mode can take place not only on the C–C bonds inside the two methyl substituents (a), but also the C–C bonds outside the groups (b). Therefore, this naphthalene-derived molecule presents four C–C bonds that would facilitate the metallocyclobutane mechanism to obtain high CN products and only two C–C bonds that involve the dicarbene path (c) to produce low CN molecules. Nevertheless, the former could be present only when either the lower-energy dicarbene path was blocked or the metallocyclobutane pathway is selectively catalyzed.

In the present work we observe that the addition of K ions to Ir/SiO_2 catalyst up to about 2–3 K-atoms nm^{-2} not only decreases the Ir particle size, but also contributes positively to the selective ring opening of sterically hindered C–C bonds. Therefore, one can tune the selectivity to ring-opening reaction just changing the potassium loading. We propose that the addition of potassium ions improve the dispersion of Ir on SiO_2 surface because of KO_x moisture–Ir interaction, eliminating the large ensembles of contiguous atoms. This is reflected in the suppression of dicarbene intermediates and the enhancement of the metallocyclobutane adsorption mode, particularly for the desirable primary product 2-MC7 (highest CN) because of the inhibition of its secondary hydrogenolysis reaction. Resasco and co-worker recently reported that high-temperature reduction on Ir catalysts is an additional way to hinder this secondary reaction [20]. Simultaneously, a lineal reduction of the ring opening activity with increasing potassium loading is observed. This inverse trend between the 1,3-DMCH conversion and the iridium-cluster size suggests that there are many fewer active sites than surface atoms on the small particles [50] and reveals the true structure sensitivity of the ring-opening reaction. Indeed, Ponec and co-workers [51] found out that the particle size does not affect significantly the ring-opening reactions over Ir catalysts, in contrast with the behavior of Pt [12]. However, Ir became more selective toward ring opening at substituted (tertiary) carbon centers as the catalyst became covered by carbonaceous species. It is possible that carbonaceous deposit can hide the true structure sensitivity of these reactions. In the present study, we found strong evidences that the particle size plays a very important role in the selectivity to substituted C–C bond rupture compared with unsubstituted C–C bonds under catalytic condition where low rate of coke formation and negligible catalyst deactivation were obtained.

4. Conclusions

The following concluding remarks can be drawn from this study:

(1) The addition of potassium ions to Ir/SiO_2 catalyst produce severe structural and superficial changes that are reflected not only on its reducibility, but also on its ability for catalyzing the ring-opening reaction of 1,3-dimethylcyclohexane and the selectivity to primary product from substituted to unsubstituted C–C cleavages. Potassium loadings up to 1–2 atoms nm^{-2} promote the reducibility of iridium oxide, probably due to its interaction with KO_x moistures that would facilitates the dissociative adsorption of hydrogen. Above potassium contents block most of the IrO_x clusters and inhibit the reduction of the catalyst precursor. Ir dispersions, on the other hand, slightly increased (as particle size decreased) with rising K surface density up to 3.1 atoms nm^{-2}, but strongly decreased at higher K loadings due to the non-uniform decorative effect of potassium over Ir particles.

(2) The ring-opening reaction of 1,3-dimethylcyclohexane over Ir/SiO_2 catalyst can be tuned with addition of potassium ions. The favorable catalytic reaction pathway on Ir/SiO_2 catalysts is the dicarbene adsorption mode, which is based on the rupture of unsubstituted C–C bond (secondary–secondary) toward products with high degrees of branching and low CNs. The addition of K ions to Ir/SiO_2 catalysts (up to 3 atoms nm^{-2}), on the other hand, markedly improves not only the Ir dispersion, but also the metallocyclobutane adsorption mode. This facilitates the cleavage of substituted C–C bonds and therefore the selectivity toward highly unbranched products with high CNs.

Acknowledgements

The authors thank to Professor D.E. Resasco and Dr. W.E. Alvarez for fruitful discussions. This work was supported by funds provided by the Oklahoma Center for the Advancement of Science and Technology (OCAST). JRL and FRG acknowledge financial support by ANPCYT, Argentina (project 06-17492); NSF-CNPq-CONICET collaborative research agreement (CIAM project) and CONICET (project PIP 6075/05). Portions of this research were carried out at the Stanford Synchrotron Radiation Laboratory, a national

user facility operated by Stanford University on behalf of the U.S. Department of Energy, Office of Basic Energy Sciences.

References

[1] A. Stanislaus, B.H. Cooper, Catal. Rev. Sci. Eng. 36 (1994) 75.
[2] H. Du, C. Fairbridge, H. Yang, Z. Ring, Appl. Catal. A: Gen. 294 (2005) 1.
[3] G.B. McVicker, M. Daage, M.S. Touvelle, C.W. Hudson, D.P. Klein, W.C. Baird Jr., B.R. Cook, J.G. Chen, S. Hantzer, D.E.W. Vaughan, E.S. Ellis, O.C. Feeley, J. Catal. 210 (2002) 137.
[4] W.C. Baird Jr., D.P. Klein, M.S. Touvelle, J.G. Chen, US Patent 6,589,416 (2003).
[5] R.C. Santana, W.E. Alvarez, J.D. Taylor, E.L. Sughrue, D.E. Resasco, Fuel 85 (2006) 643.
[6] M. Santikunaporn, J.E. Herrera, S. Jongpatiwut, D.E. Resasco, W.E. Alvarez, E.L. Sughrue, J. Catal. 228 (2004) 100.
[7] R.J. Fenoglio, G.M. Nuñez, D.E. Resasco, J. Catal. 121 (1990) 77.
[8] D. Teschner, K. Matusek, Z. Paal, J. Catal. 192 (2000) 335.
[9] G. Del Angel, B. Coq, R. Dutartre, F. Figueras, J. Catal. 87 (1984) 27.
[10] F.J. Schepers, J.G. Van Senden, E.H. Van Broekhoven, V. Ponec, J. Catal. 94 (1985) 400.
[11] F. Weisang, F.G. Gault, J. Chem. Soc. Chem. Commun. 11 (1979) 519.
[12] F.G. Gault, Adv. Catal. 30 (1981) 1.
[13] B. Coq, E. Crabb, F. Figueras, J. Mol. Catal. A: Chem. 96 (1995) 35.
[14] T.E. Hoost, J.G. Goodwing Jr., J. Catal. 130 (1991) 283.
[15] A.M. Kazi, B. Chen, J.G. Goodwing Jr., G. Marcelin, N. Rodriguez, R.T.K. Baker, J. Catal. 157 (1995) 1.
[16] C. Pedrero, T. Waku, E. Iglesia, J. Catal. 233 (2005) 242.
[17] W.C. Baird Jr., J.G. Chen, G.B. McVicker, US Patent 6,623,626 (2003).
[18] W.C. Baird Jr., D.P. Klein, M.S. Touvelle, J.G. Chen, G.B. McVicker, US Patent 6,586,650 (2003).
[19] W.C. Baird Jr., J.G. Chen, G.B. McVicker, US Patent 6,623,625 (2003).
[20] P.T. Do, W.E. Alvarez, D.E. Resasco, J. Catal. 238 (2006) 477.
[21] G.D. Meitzner, E. Iglesia, Catal. Today 53 (1999) 433.
[22] D.G. Barton, S.L. Soled, G.D. Meitzner, G.A. Fuentes, E. Iglesia, J. Catal. 181 (1999) 57.
[23] B. Ravel, M. Newville, J. Synchrotron Rad. 12 (2005) 537.
[24] J.J. Rehr, R.C. Albers, Rev. Mod. Phys. 72 (2000) 621.
[25] B. Ravel, J. Synchrotron Rad. 8 (2001) 314.
[26] F. Locatelli, D. Uzio, G. Niccolai, J.M. Basset, J.P. Candy, Catal. Commun. 4 (2003) 189.
[27] K. Aika, K. Shimakazi, Y. Hattori, A. Ohya, S. Ohshima, K. Shirota, A. Ozaki, J. Catal. 92 (1985) 296.
[28] J.S. Rieck, A.T. Bell, J. Catal. 100 (1986) 305.
[29] M. Konsolakis, I.V. Yentekakis, Appl. Catal. B: Environ. 29 (2001) 103.
[30] K. Foger, H. Jaeger, J. Catal. 70 (1981) 53.
[31] C. Wögerbauer, M. Caciejewski, A. Baiker, U. Göbelt, J. Catal. 201 (2001) 113.
[32] M. Haneda, Y. Kintaichi, N. Bion, H. Hamada, Appl. Catal. B: Environ. 46 (2003) 473.
[33] L. Feng, X. Li, D.B. Dadyburjor, E.L. Kugler, J. Catal. 190 (2000) 1.
[34] A. Iordan, M.I. Zaki, C. Kappenstein, C. Géron, Phys. Chem. Chem. Phys. 5 (2003) 1708.
[35] J.S. Rieck, A.T. Bell, J. Catal. 99 (1986) 278.
[36] R.P. Underwood, A.T. Bell, J. Catal. 109 (1988) 61.
[37] C.D. Wagner, A.V. Naumkin, A. Kraut-Vass, J.W. Allison, C.J. Powell, J.R. Rumble Jr., NIST X-ray Photoelectron Spectroscopy Database (NIST Standard Reference Database 20, Web Version 3.4).
[38] L.F. Liotta, G. Deganello, C. Leclercq, G.A. Martin, J. Catal. 164 (1996) 334.
[39] L.F. Liotta, A.M. Venezia, A. Martorana, G. Deganello, J. Catal. 171 (1997) 177.
[40] A. Cimino, D. Gazzoli, M. Valigi, J. Electron Spectrosc. Relat. Phenom. 104 (1999) 1.
[41] P. Reyes, M.C. Aguirre, I. Melian-Cabrera, M. Lopez Granados, J.L.G. Fierro, J. Catal. 208 (2002) 229.
[42] T. Marzialetti, J.L.G. Fierro, P. Reyes, Catal. Today 107–108 (2005) 235.
[43] A.I. Frenkel, C.W. Hills, R.G. Nuzzo, J. Phys. Chem. B 105 (2001) 12689.
[44] A. Balerna, S. Mobilio, Phys. Rev. B 34 (1986) 2293.
[45] D. Zanchet, H. Tolentino, M. Martins Alves, O. Alves, D. Ugarte, Chem. Phys. Lett. 323 (2000) 167.
[46] M.F. Wilson, I.P. Fisher, J.F. Kriz, Ind. Eng. Chem. Prod. Res. Dev. 25 (1986) 505.
[47] K. Foger, J.R. Anderson, J. Catal. 59 (1979) 325.
[48] M. Boudart, L.D. Ptak, J. Catal. 15 (1970) 90.
[49] V. Amir-Ebrahimi, A. Choplin, P. Parayre, F.G. Gault, Nouv. J. Chem. 4 (1980) 431.
[50] F.H. Ribeiro, A.E. Schach Von Wittenau, C.H. Bartholomew, G.A. Somorjai, Catal. Rev. Sci. Eng. 39 (1997) 49.
[51] J.G. van Senden, E.H. van Broekhoven, J. Vreesman, V. Ponec, J. Catal. 87 (1984) 468.